New Cation–Anion Interaction Motifs, Electronic Band Structure, and Electrical Behavior in β-$(ET)_2X$ Salts (X = ICl_2^- and $BrICl^-$)

Thomas J. Emge,[†] Hau H. Wang,[†] Peter C. W. Leung,[†] Paul R. Rust,[†] Jan D. Cook,[†] Patricia L. Jackson,[†] K. Douglas Carlson,[†] Jack M. Williams,*[†] Myung-Hwan Whangbo,*[‡] Eugene L. Venturini,[§] James E. Schirber,[§] Larry J. Azevedo,[§] and John R. Ferraro[⊥]

Contribution from the Chemistry and Materials Science and Technology Divisions, Argonne National Laboratory, Argonne, Illinois 60439, Department of Chemistry, North Carolina State University, Raleigh, North Carolina 27650, Sandia National Laboratories, Albuquerque, New Mexico 87185, and Department of Chemistry, Loyola University, Chicago, Illinois 60626. *Received September 12, 1985*

Abstract: Two new organic metals, β-$(ET)_2ICl_2$ and β-$(ET)_2BrICl$, were synthesized, and their structures and electronic properties were characterized via X-ray diffraction, ESR studies, and band electronic structure calculations. BEDT-TTF, abbreviated "ET", is bis(ethylenedithio)tetrathiafulvalene, $C_{10}S_8H_8$. The packing of the ET molecules within the sheetlike network of these two isostructural salts is significantly different from that of the two-dimensional metals β-$(ET)_2X$ with the larger anions $X^- = I_3^-$, I_2Br^-, IBr_2^-, and AuI_2^-, where all but $X^- = I_2Br^-$ are ambient-pressure superconductors. The ESR studies for the β-$(ET)_2ICl_2$ salt show that it is metallic down to ~22 K, at which temperature a metal–insulator transition is observed. The band electronic structures calculated for β-$(ET)_2ICl_2$ and β-$(ET)_2BrICl$ reveal that these salts are one-dimensional metals. Comparison of the structures and electronic properties of the β-$(ET)_2X$ salts with large linear anions (e.g., $X^- = I_3^-$, I_2Br^-, IBr_2^-, and AuI_2^-) vs. those with the small symmetric $(Cl–I–Cl)^-$ and asymmetric $(Br–I–Cl)^-$ anions leads us to conclude that the nature of the interactions between ET molecules within a given sheetlike network, and hence the dimensionality of electrical properties, is strongly governed by the packing motif of ET molecules around a particular X^- anion.

The new synthetic metals β-$(BEDT\text{-}TTF)_2X$, where X^- is a linear monovalent anion and BEDT-TTF (also known as ET) is the radical cation bis(ethylenedithio)tetrathiafulvalene **1**, have

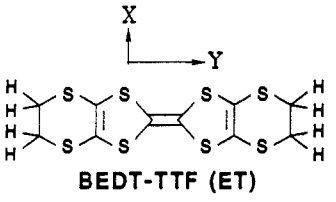

1

been of much interest recently.[1-3] The initial discovery of ambient-pressure superconductivity in β-$(ET)_2I_3$ (T_c = 1.4 K)[4-7] has been followed by that in β-$(ET)_2IBr_2$ (T_c = 2.7 K)[8,9] and β-$(ET)_2AuI_2$ (T_c = ~5.0 K).[10] The crystallographic *ab* plane of these compounds contains a sheetlike network of ET molecules,[5,7,8,10] which is made up of interacting ET stacks linked through extensive S···S interactions that constitute the electron conduction pathway in these systems. Along the *c* axis of the β-$(ET)_2X$ structures, separate layers of the ET molecules and X^- anion sheets alternate. Corresponding to these structural features, these organic salts are two-dimensional (2D) metals with high electrical conductivity in all directions within the *ab* plane.[4,11,12] The 2D packing motif of ET molecules mentioned above is frequently encountered in other $(ET)_mX_n$ salts. For example, there are several different phases of $(ET)_2I_3$[5,13] and many different stoichiometries of $(ET)_m(ReO_4)_n$ salts, such as $(ET)_2ReO_4$,[14a] $(ET)_2(ReO_4)(THF)_{0.5}$,[14b] and $(ET)_3(ReO_4)_2$.[15] Whether or not such 2D networks lead to 2D or 1D metallic properties depends on the relative magnitudes of various interactions between the ET molecules within a given network.

Most $(ET)_mX_n$ salts with nonlinear anions ($X^- = ReO_4^-$, BrO_4^-, ClO_4^-, PF_6^-) seem to exhibit 1D metallic properties[3,14,16-18] and are susceptible to metal–insulator (MI) transitions, as found, for example, in β-$(ET)_2PF_6$ at 297 K[18] and $(ET)_3(ClO_4)_2$ at 170 K.[3] In contrast, β-$(ET)_2X$ salts with long, linear anions ($X^- = I_3^-$,

[†] Argonne National Laboratory.
[‡] North Carolina State University.
[§] Sandia National Laboratories.
[⊥] Loyola University.

(1) Williams, J. M.; Beno, M. A.; Wang, H. H.; Leung, P. C. W.; Emge, T. J.; Geiser, U.; Carlson, K. D. *Acc. Chem. Res.* **1985**, *18*, 261.
(2) Leung, P. C. W.; Beno, M. A.; Emge, T. J.; Wang, H. H.; Bowman, M. K.; Firestone, M. A.; Sowa, L. M.; Williams, J. M. *Mol. Cryst. Liq. Cryst.* **1985**, *125*, 113.
(3) Kobayashi, H.; Kato, R.; Mori, T.; Kobayashi, A.; Sasaki, Y.; Saito, G.; Enoki, T.; Inokuchi, H. *Mol. Cryst. Liq. Cryst.* **1984**, *107*, 33.
(4) Yagubskii, E. B.; Shchegolev, I. F.; Laukhin, V. N.; Kononovich, P. A.; Kartsovnik, A. V.; Zvarykina, A. V.; Buravov, L. I. *Pis'ma Zh. Eksp. Teor, Fiz.* **1984**, *39*, 12; *JETP Lett. (Engl. Transl.)* **1984**, *39*, 12.
(5) Shibaeva, R. P.; Kaminskii, V. F.; Yagubskii, E. B. *Mol. Cryst. Liq. Cryst.* **1985**, *119*, 361.
(6) Crabtree, G. W.; Carlson, K. D.; Hall, L. N.; Copps, P. T.; Wang, H. H.; Emge, T. J.; Beno, M. A.; Williams, J. M. *Phys. Rev. B: Condens. Matter* **1984**, *30*, 2958.
(7) Williams, J. M.; Emge, T. J.; Wang, H. H.; Beno, M. A.; Copps, P. T.; Hall, L. N.; Carlson, K. D.; Crabtree, G. M. *Inorg. Chem.* **1984**, *23*, 2558.
(8) Williams, J. M.; Wang, H. H.; Beno, M. A.; Emge, T. J.; Sowa, L. M.; Copps, P. T.; Behroozi, F.; Hall, L. N.; Carlson, K. D.; Crabtree, G. W. *Inorg. Chem.* **1984**, *23*, 3839.
(9) Carlson, K. D.; Crabtree, G. W.; Hall, L. N.; Behroozi, F.; Copps, P. T.; Sowa, L. M.; Nuñez, L.; Firestone, M. A.; Wang, H. H.; Beno, M. A.; Emge, T. J.; Williams, J. M. *Mol. Cryst. Liq. Cryst.* **1985**, *125*, 159.
(10) (a) Wang, H. H.; Beno, M. A.; Geiser, U.; Firestone, M. A.; Webb, K. S.; Nuñez, L.; Crabtree, G. W.; Carlson, K. D.; Williams, J. M.; Azevedo, L. J.; Kwak, J. F.; Schirber, J. E. *Inorg. Chem.* **1985**, *24*, 2465. (b) Carlson, K. D.; Crabtree, G. W.; Nuñez, L.; Wang, H. H.; Beno, M. A.; Geiser, U.; Firestone, M. A.; Webb, K. S.; Williams, J. M. *Solid State Commun.* **1986**, *57*, 89.
(11) Carlson, K. D.; Crabtree, G. W.; Hall, L. N.; Copps, P. T.; Wang, H. H.; Emge, T. J.; Beno, M. A.; Williams, J. M. *Mol. Cryst. Liq. Cryst.* **1985**, *119*, 357.
(12) Tokumoto, M.; Anzai, H.; Bando, H.; Saito, G.; Kinoshita, N.; Kajimura, K.; Ishiguro, T. *J. Phys. Soc. Jpn.* **1985**, *54*, 869.
(13) (a) Bender, K.; Dietz, K.; Endres, H.; Helberg, H. W.; Henning, I.; Keller, H. J.; Schäfer, H. W.; Schweitzer, D. *Mol. Cryst. Liq. Cryst.* **1984**, *107*, 45. (b) Schwenk, H.; Gross, F.; Heidmann, C.-P.; Andres, K.; Schweitzer, D.; Keller, H. *Mol. Cryst. Liq. Cryst.* **1985**, *119*, 329. (c) Koch, B.; Geserich, H. P.; Ruppel, W.; Schweitzer, D.; Dietz, K. H.; Keller, H. J. *Mol. Cryst. Liq. Cryst.* **1985**, *119*, 343. (d) Bender, K.; Hennig, I.; Schweitzer, D.; Dietz, K.; Endres, H.; Keller, H. J. *Mol. Cryst. Liq. Cryst.* **1984**, *108*, 359.
(14) (a) Parkin, S. S. P.; Engler, E. M.; Schumaker, R. R.; Lagier, R.; Lee, V. Y.; Scott, J. C.; Greene, R. L. *Phys. Rev. Lett.* **1983**, *50*, 270. (b) Parkin, S. S. P.; Engler, E. M.; Lee, V. Y.; Schumaker, R. R. *Mol. Cryst. Liq. Cryst.* **1985**, *119*, 375.

0002-7863/86/1508-0695$01.50/0

Table I. IR and Raman Spectral Data for Solid $(R_4N)X$ Salts with $X^- = ICl_2^-$, IBr_2^-, and $BrICl^-$ [a]

	$(Et_4N)ICl_2$[b]		$(n\text{-}Bu_4N)IBr_2$[b]		$(n\text{-}Bu_4N)ICl_2$[c]		$(n\text{-}Bu_4N)BrICl$[c]	
vibrational mode, cm^{-1}	IR	Raman	IR	Raman	IR	Raman	IR	Raman
ν_1 symmetric stretching	260 (sh)	261, 257, 253[d]		168[e]	266 (m)	257 (vs)		257 (w), 157 (s)
ν_2 bending	126		65		126, 113 (m)		116, 113 (m)	
ν_3 asymmetric stretching	214		169		221 (vs)	212 (vw)	229 (s), 221 (s), 171 (s)	232 (w)

[a] Symbols are s, strong; m, medium; w, weak; v, very, sh, shoulder. Assignments of vibrational modes made on basis of a linear symmetry [D_{3h} for $(n\text{-}Bu_4N)ICl_2$ and $(n\text{-}Bu_4N)IBr_2$ and $C_{\infty v}$ for $(n\text{-}Bu_4N)BrICl$]. [b] Reference 25b. [c] Reference 24. [d] The triplet is due to isotopic resonances. [e] Our data[24] for $(n\text{-}Bu_4N)IBr_2$ show strong absorption in the IR at 166 cm^{-1} with a weak feature at 138 cm^{-1} and a strong 168 cm^{-1} peak in the Raman. The assignments for $(n\text{-}Bu_4N)BrICl$ are tentative.

I_2Br^-, IBr_2^-, AuI_2^-)[4,11,12,19,20] are all 2D metals and except for $X^- = I_2Br^-$ are ambient-pressure superconductors. Also, α-$(ET)_2I_3$ is 2D metallic above 135 K.[13] Recently, we have studied the effect of systematically varying the size of the linear anions ($X^- = I_3^-$, I_2Br^-, IBr_2^-) upon the intermolecular separations between ET molecules within a 2D network[19,21] and also its effect upon the magnitudes of interactions between the ET molecules.[22] These studies indicate (i) that a decrease in anion length in the β-$(ET)_2X$ series generally brings the ET molecules closer together within the network, and (ii) that consideration of H···X^- interactions, which are present between ET molecules and X^- anions, is very important for the understanding of overall crystal packing.

It may be possible to decrease the size of a linear anion, X^-, to such a point that the intermolecular interactions within the resulting ET network promote 1D metallic properties in the corresponding $(ET)_2X$ salt because of disruption of the 2D ET molecular system. Such is the case for the β-$(ET)_2X$ salts with $X^- = ICl_2^-$ and $BrICl^-$ that have been synthesized and characterized in this study. The anions $(Cl\text{-}I\text{-}Cl)^-$ and $(Br\text{-}I\text{-}Cl)^-$ have effective lengths (including the van der Waals radii of the terminal atoms Br or Cl) that are ~1.4 and ~1.1 Å shorter than the I_3^- anion (at 10.1 Å), respectively.

In the present work, we describe the crystal and band electronic structures of β-$(ET)_2ICl_2$ and β-$(ET)_2BrICl$ and the electrical behavior based on ESR studies of β-$(ET)_2ICl_2$. Also, the compositions and geometries of the $X^- = ICl_2^-$ and $BrICl^-$ anions in these salts were further studied by analyzing polycrystalline samples of $(n\text{-}Bu_4N)X$ (the supporting electrolyte in their crystallization) via IR and Raman techniques. The packing of ET molecules in the structures of these β-$(ET)_2X$ salts with small linear anions, ICl_2^- and $BrICl^-$ is different from that in salts with the large linear anions ($X^- = I_3^-$, I_2Br^-, IBr_2^-, AuI_2^-), and the effects on the electrical properties are described herein. The present ESR study shows that β-$(ET)_2ICl_2$ is metallic down to ~22 K, at which temperature this compound undergoes a metal–insulator (MI) transition. The band electronic structures calculated for the isostructural salts β-$(ET)_2ICl_2$ and β-$(ET)_2BrICl$ show that they are 1D metals, which is consistent with the ESR results on β-$(ET)_2ICl_2$.

Synthesis of $(n\text{-}Bu_4N)BrICl$

Initially, 100 mL of absolute ethanol was purged with argon for 10 min. Then, 5.3 g of $(n\text{-}Bu_4N)Cl$ (Aldrich, 19.1 mmol) was dissolved in the alcohol and 4.1 g of IBr (Aldrich, 19.9 mmol) was quickly added to the solution. The red-orange solution was stirred for 20 min and heated to boiling and then hot filtered. The filtrate was concentrated, cooled slowly, and stored in a refrigerator to give 8.1 g of crude product. The crude product was recrystallized twice from absolute ethanol to yield 6.8 g of $(n\text{-}Bu_4N)BrICl$ (73%): mp 74–75 °C; Anal. Calcd (found, Midwest Microlab, Indianapolis, IN) for $C_{16}H_{36}NBrICl$: C, 39.65 (39.43); H, 7.49 (7.70); N, 2.89 (3.06); I, 26.18 (26.09).

Synthesis of $(n\text{-}Bu_4N)ICl_2$

A similar procedure was undertaken to prepare $(n\text{-}Bu_4N)ICl_2$, except that the reaction was carried out in an ice–water bath to avoid heating. Thus, 5.0 g of $(n\text{-}Bu_4N)Cl$ (18.0 mmol) reacted with 3.0 g of ICl (Aldrich, 18.4 mmol) in 100 mL of absolute ethanol to give 6.45 g of bright yellow product. Two recrystallizations from cold, absolute ethanol yielded 3.97 g of pure $(n\text{-}Bu_4N)ICl_2$ (50%): mp 67–69 °C; Anal. Calcd (found) for $C_{16}H_{36}NICl_2$: C, 43.65 (43.52); H, 8.24 (8.43); N, 3.18 (2.91); I, 28.82 (28.73).

Crystallization of β-$(ET)_2ICl_2$ and β-$(ET)_2BrICl$

Both electrocrystallizations were carried out according to the literature procedure.[7] For the synthesis of the $(ET)_2BrICl$ crystals, the solution of supporting electrolyte that was needed for the electrochemical cell consisted of 0.33 g of $(n\text{-}Bu_4N)BrICl$ in 10 mL of dry THF and 10.6 mg of ET (Strem Chemical Co.) in 5 mL of dry THF. After 7 days at constant current density (0.64 $\mu A/cm^2$) and temperature (23.0 ± 0.2 °C), 4.9 mg of shiny black needles of $(ET)_2BrICl$ salts were harvested (35% yield) in addition to a minor amount of polycrystalline precipitate. Single crystals were surveyed by means of an ESR technique,[2] and each crystal examined had a peak-to-peak line width in one of two ranges. Crystals with a line width of ~50 Oe were later characterized by X-ray diffraction as the α-phase and those with a line width of ~10 Oe were found to be the β-phase (vide infra).

For the synthesis of the $(ET)_2ICl_2$ crystals, a constant current density of 1.0 $\mu A/cm^2$ and a constant temperature of 22.3 ± 0.2 °C were used. The solutions used for the cell consisted of 1.21 g of $(n\text{-}Bu_4N)ICl_2$ in 30 mL of dry THF and 33.5 mg of ET in 15 mL of dry THF. After 1 week of crystal growth, 8.35 mg of β-$(ET)_2ICl_2$ were harvested from the anode (20% yield). Additionally, black polycrystalline material precipitated from the anode solution. The only phase found among these crystals was β-$(ET)_2ICl_2$, which has a line width of ~10 Oe.

IR and Raman Spectra of $(n\text{-}Bu_4N)X$, $X^- = ICl_2^-$ and $BrICl^-$

The "$BrICl^-$" anions of β-$(ET)_2BrICl$ are introduced by way of $(n\text{-}Bu_4N)BrICl$ in the electrocrystallization of this organic metal. To characterize the composition of the $BrICl^-$ species prepared as described above, we examined the IR and Raman spectra of polycrystalline samples of $(n\text{-}Bu_4N)X$ ($X^- = ICl_2^-$, IBr_2^-, or $BrICl^-$) according to a previously described procedure.[24] The measured frequencies of the symmetric stretching (ν_1), the doubly degenerate bending (ν_2), and asymmetric stretching (ν_3) modes of the above three trihalide anions are listed in Table I, and the corresponding data of Gabes and Gerding[25b] for solid samples of $(Et_4N)ICl_2$ and $(n\text{-}Bu_4N)IBr_2$ are also included for comparison. The ν_1, ν_2, and ν_3 frequencies of $(n\text{-}Bu_4N)ICl_2$ are similar to those of $(Et_4N)ICl_2$.[25b] Since the ν_1 mode is active in the IR, the ICl_2^- anions in these alkylammonium salts are not exactly linear. In contrast, the IBr_2^- anions in $(n\text{-}Bu_4N)IBr_2$ are linear.[24,25b] It is noted that some of the frequencies of both IBr_2^- and ICl_2^- are found for the $BrICl^-$ in $(n\text{-}Bu_4N)BrICl$ within experimental error

(15) Kobayashi, H.; Kobayashi, A.; Sasaki, Y.; Saito, G.; Inokuchi, H. *Chem. Lett.* **1984**, 183.
(16) Williams, J. M.; Beno, M. A.; Wang, H. H.; Reed, P. E.; Azevedo, L. J.; Schirber, J. E. *Inorg. Chem.* **1984**, *23*, 1790.
(17) Kobayashi, H.; Kobayashi, A.; Sasaki, Y.; Saito, G.; Enoki, T.; Inokuchi, H. *J. Am. Chem. Soc.* **1983**, *105*, 209.
(18) Kobayashi, H.; Mori, T.; Kato, R.; Kobayashi, A.; Sasaki, Y.; Saito, G.; Inokuchi, H. *Chem. Lett.* **1983**, 581.
(19) (a) Emge, T. J.; Wang, H. H.; Beno, M. A.; Leung, P. C. W.; Firestone, M. A.; Jenkins, H. C.; Cook, J. D.; Carlson, K. D.; Williams, J. M.; Venturini, E. L.; Azevedo, L. J.; Schirber, J. E. *Inorg. Chem.* **1985**, *24*, 1736. (b) Emge, T. J.; Leung, P. C. W.; Beno, M. A.; Wang, H. H.; Firestone, M. A.; Webb, K. S.; Carlson, K. D.; Williams, J. M.; Venturini, E. L.; Azevedo, L. J.; Schirber, J. E. *Mol. Cryst. Liq. Cryst.* **1986**, *132*, 363.
(20) Jacobsen, C. S.; Williams, J. M.; Wang, H. H. *Solid State Commun.* **1985**, *54*, 937.
(21) Beno, M. A.; Emge, T. J.; Firestone, M. A.; Sowa, L. M.; Wang, H. H.; Williams, J. M.; Whangbo, M.-H. to be published.
(22) Whangbo, M.-H.; Williams, J. M.; Leung, P. C. W.; Beno, M. A.; Emge, T. J.; Wang, H. H. *Inorg. Chem.* **1985**, *24*, 3500.
(23) Wells, A. F. "Structural Inorganic Chemistry", 5th ed.; Oxford University Press: New York, 1984; p 396.
(24) Ferraro, J. R.; Beno, M. A.; Thorn, R. J.; Wang, H. H.; Webb, K. S.; Williams, J. M. *J. Phys. Chem. Solids*, in press.
(25) (a) Maki, A. G.; Forneris, R. *Spectrochim. Acta, Part A* **1967**, *23A*, 867. (b) Gages, W.; Gerding, H. *J. Mol. Struct.* **1972**, *14*, 267.

Table II. Unit Cell and Data Collection Parameters for β-(ET)$_2$ICl$_2$ and β-(ET)$_2$BrICl at 298/120 K

	β-(ET)$_2$ICl$_2$[a]		β-(ET)$_2$BrICl[b]	
	298 K	120 K	298 K	120 K
a, Å	6.645 (1)	6.620 (1)	6.642 (1)	6.616 (1)
b, Å	9.771 (1)	9.638 (2)	9.816 (2)	9.668 (2)
c, Å	12.921 (2)	12.859 (3)	12.975 (2)	12.919 (2)
α, deg	87.19 (1)	86.47 (2)	87.29 (2)	86.60 (1)
β, deg	100.91 (1)	101.33 (2)	101.11 (2)	101.64 (1)
γ, deg	98.63 (1)	97.77 (2)	98.28 (1)	97.32 (1)
V, Å^3	814.3 (2)	796.5 (3)	821.3 (2)	802.4 (2)
d_c, g cm^{-3}	1.972	2.016	2.044	2.092
T_{min}, T_{max}	0.64, 0.84		0.58, 0.86	
μ, cm^{-1}	21.4	21.9	32.5	33.0
2θ Mo Kα, deg	0–60	0–60[c]	0–55	0–60[d]
no. data collect.	5464	5622	4276	6216
no. obsd ($F > 0$)	4538	4111	3636	4014
excursions (*e* Å)	±1.5	±1.2	±2.0	±2.1
$R(F)$[e]	0.037	0.022	0.048	0.044
$R_w(F)$	0.030	0.025	0.047	0.048
GOF	1.81	1.73	2.79	3.83

[a] Space group $P\bar{1}$ (Z = 1). Crystal dimensions are 0.26 × 0.23 × 0.08 mm along [1$\bar{1}$0], [010], and [001]. [b] Space group $P\bar{1}$ (Z = 1). Crystal dimensions are 0.33 × 0.27 × 0.04 mm along [100], [011], and [01$\bar{1}$]. [c] Includes full sphere of diffraction data to 35°, but some data in the region 45° < 2θ < 55° were not collected because of a failure with the low-temperature apparatus. [d] Includes full sphere to 55°. [e] $R(F) = [\Sigma||F_o| - ||F_c||/\Sigma|F_o|]$; $R_w(F) = [\Sigma w(|F_o| - |F_c|)^2/\Sigma wF_o^2]^{1/2}$; GOF = $[\Sigma w(|F_o| - |F_c|)^2/(n - m)]^{1/2}$, for n observed data and m = 178 variables.

(some decomposition of the samples under the argon laser, 5145 Å, occurred for the Raman measurements). Similar results have been obtained for $(CH_3)_4NBrICl$ by Maki and Forneris.[25a] This strongly suggests that (n-Bu$_4$N)BrICl contains both IBr_2^- and ICl_2^- anions, although the absence of $(Br-I-Cl)^-$ anions cannot be concluded from these data alone. As noted previously,[19a] the halide with the highest atomic number always resides in the center for mixed trihalides.[23] Consequently, the β-(ET)$_2$BrICl salt used in our X-ray diffraction analysis may contain a mixture of the above three ions. Because of geometry and symmetry requirements, the relative compositions of these anions cannot be derived on the basis of the structural data presented here. Thus, we will ascribe the notation and stoichiometry $BrICl^-$ to the mixture of these three anions in β-(ET)$_2$BrICl.

X-ray Diffraction Data

Flat hexagons of β-(ET)$_2$ICl$_2$ and β-(ET)$_2$BrICl crystals were selected for X-ray diffraction data collection. Unit cell and data collection parameters and final refinement agreement factors for the isostructural salts of β-(ET)$_2$ICl$_2$ and β-(ET)$_2$BrICl at 298 and 120 K are presented in Table II. Based on ESR[2] and X-ray diffraction data from many samples, only the β-phase of (ET)$_2$ICl$_2$ and the α- and β-phases of (ET)$_2$BrICl have been identified. The α-(ET)$_2$BrICl salt is isostructural to α-(ET)$_2$IBr$_2$,[21] which has a unit cell volume of ~1600 Å^3. The β-phase has been assigned to the triclinic phases of (ET)$_2$X salts with $X^- = I_3^-$, IBr_2^-, and I_2Br^-[1-3] and herein to those with $X^- = ICl_2^-$ and $BrICl^-$, which all have unit cell volumes of ~800 Å^3.

Intensity data were collected on a Syntex P2$_1$ diffractometer, equipped with a LN_2-cooled low-temperature device. Each θ–2θ scan began 1.2° before the Mo Kα1 diffracted beam and ended 1.3° above Mo Kα2, with a constant background/scan time ratio of 1/2. During the course of each experiment, two standard reflections were monitored after every 94 reflections, and no significant variations in their intensities were observed. Corrections for Lorentz effects, polarization, and absorption were applied to all data. Further details of the diffraction experiments are included in Table II. All nonhydrogen atoms were located after initial structure factor and difference-density syntheses that included only the I atom at the origin (0,0,0). At an intermediate point in the least-squares refinement using the 120 K data, a difference-density synthesis was used to locate all H atoms, which were near their calculated positions in all cases. The fixed distance of 1.09 Å for each C–H bond used here represents the internuclear distance based on neutron diffraction data.[26] Neutral atom scattering factors including correction terms for anomalous dispersion were taken from the "International Tables for X-ray Crystallography". Table III lists the fractional coordinates and equivalent thermal parameters (U_{eq}) for the nonhydrogen atoms in β-(ET)$_2$ICl$_2$ and β-(ET)$_2$BrICl at 298 and 120 K.

We noted above that the possibility of a mixture of ICl_2^-, IBr_2^-, and $BrICl^-$ anions and, therefore, anion disorder in the β-(ET)$_2$BrICl salt exist. In the crystal structures of β-(ET)$_2$ICl$_2$ and β-(ET)$_2$IBr$_2$,[8] the I–Cl and I–Br bond lengths differ only by 0.1 Å. On the basis of the electron density map, the I–Br and I–Cl bonds are alinged along the same direction in the crystal structure of β-(ET)$_2$BrICl. Therefore, the positions of the Br and Cl atoms, which alternate randomly throughout the structure, are nearly superimposable. Due to high correlations between occupancy factors and the positional and thermal parameters of the Br and Cl atoms, their occupancies were not varied but were assigned to values of $^1/_2$. Despite the probable mixture of the three different anions in β-(ET)$_2$BrICl, the ET molecule network is completely *ordered*, just as in β-(ET)$_2$ICl$_2$. The implication of this similarity of ET networks will be discussed later.

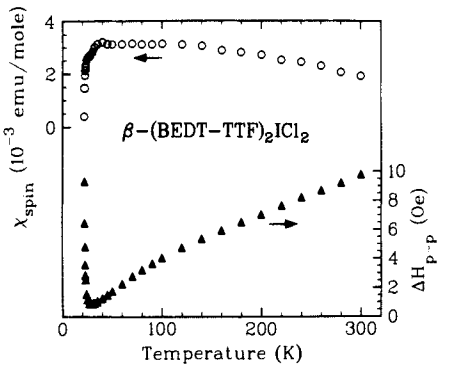

Figure 1. Single-crystal ESR data from 20 to 300 K for β-(ET)$_2$ICl$_2$ are evidence of an MI transition at ~22 K, which is attributed to a spin density wave (SDW) (see text). Open circles at the top represent the spin susceptibility of the sample with the applied magnetic field along the c^* axis. Solid triangles at the bottom represent peak-to-peak line widths (Oe).

ESR Measurements

Shown in Figure 1 are the electron spin resonance (ESR) data derived from a single crystal of β-(ET)$_2$ICl$_2$ measured from 20 to 300 K. Due to anion disorder in β-(ET)$_2$BrICl, superconductivity is not expected, and its electrical and ESR behavior is predicted to mimic that of β-(ET)$_2$I$_2$Br, i.e., dominated by the anion disorder.[19a] The data were recorded with a conventional homodyne spectrometer at 9.8 GHz with a helium gas flow refrigerator and a rectangular microwave cavity. The sample was held by gravity in a narrow slot cut in a small Teflon holder (no grease or cement was used on the sample to avoid all stresses at low temperatures). A thin-plate crystal used for these measurements weighed 125 μg and measured approximately 0.5 × 0.8 × 0.1 mm. The derivative ESR line shape had an A/B ratio of unity (completely symmetric) at all temperatures when the microwave magnetic field was aligned in the plane of the sample. This indicates low conductivity along at least one direction normal to the microwave magnetic field which was parallel to the plane of the sample.

The open circles at the top of Figure 1 show the spin susceptibility with the static applied magnetic field normal to the plate directions of the sample (i.e., along the crystallographic c^* axis) and with the microwave magnetic field in the plane of the plate. The susceptibility rises gradually from 2 × 10^{-3} emu/mol at room temperature to 3 × 10^{-3} emu/mol near 100 K and remains constant down to 40 K. It then decreases to 2 × 10^{-3} emu/mol at

(26) Taylor, R.; Kennard, O. *Acc. Chem. Res.* **1984**, *17*, 320 and references therein.

Table III. Final Non-Hydrogen Atomic Fractional Coordinates and Equivalent Thermal Parameters ($U_{eq} \times 10^4$)

A. β-$(ET)_2ICl_2$ at 120/298 K

atom	x	y	z	U_{eq}[a]	atom	x	y	z	U_{eq}[a]
I	0.0000	0.0000	0.0000	149 (1)	C1	0.1399 (3)	−0.2834 (2)	0.49215 (13)	127 (5)
	0.0000	0.0000	0.0000	351 (1)		0.1435 (3)	−0.2833 (2)	0.4926 (2)	271 (6)
Cl	0.08441 (7)	0.23683 (4)	−0.09315 (3)	191 (1)	C2	0.0392 (3)	−0.3699 (2)	0.41247 (13)	128 (5)
	0.08878 (11)	0.23412 (7)	−0.08999 (5)	455 (2)		0.0426 (3)	−0.3697 (2)	0.4127 (2)	268 (6)
S1	0.40757 (7)	−0.26978 (4)	0.53756 (3)	143 (1)	C3	0.4136 (3)	−0.1453 (2)	0.63220 (13)	148 (5)
	0.40956 (9)	−0.26840 (7)	0.53739 (5)	328 (2)		0.4159 (4)	−0.1438 (3)	0.6311 (2)	322 (7)
S2	0.00886 (7)	−0.17690 (4)	0.55391 (3)	148 (1)	C4	0.2306 (3)	−0.1033 (2)	0.64094 (13)	134 (5)
	0.01472 (9)	−0.17775 (6)	0.55385 (5)	336 (2)		0.2365 (4)	−0.1024 (2)	0.6398 (2)	285 (6)
S3	0.17092 (7)	−0.47101 (4)	0.34687 (3)	143 (1)	C5	−0.0491 (3)	−0.5357 (2)	0.25390 (12)	128 (5)
	0.17177 (9)	−0.47021 (6)	0.34713 (5)	320 (2)		−0.0481 (4)	−0.5339 (2)	0.2544 (2)	278 (6)
S4	−0.22899 (7)	−0.38510 (4)	0.36821 (3)	143 (1)	C6	−0.2322 (3)	−0.4964 (2)	0.26500 (13)	126 (5)
	−0.22376 (9)	−0.38574 (6)	0.36928 (5)	323 (2)		−0.2268 (3)	−0.4951 (2)	0.2654 (2)	268 (6)
S5	0.66086 (7)	−0.08502 (5)	0.70354 (4)	218 (1)	C7	0.6094 (3)	0.0885 (2)	0.73104 (15)	187 (6)
	0.66252 (10)	−0.08310 (9)	0.70242 (7)	531 (3)		0.6157 (5)	0.0881 (3)	0.7301 (2)	425 (9)
S6	0.18163 (7)	0.01963 (5)	0.72470 (4)	185 (1)	C8	0.4415 (3)	0.0827 (2)	0.79605 (14)	189 (6)
	0.18899 (11)	0.01935 (7)	0.72348 (6)	429 (2)		0.4459 (5)	0.0840 (3)	0.7934 (2)	422 (9)
S7	−0.00248 (7)	−0.64208 (5)	0.15777 (3)	173 (1)	C9	−0.2377 (3)	−0.6293 (2)	0.05929 (14)	191 (6)
	−0.00171 (10)	−0.63941 (7)	0.15844 (5)	413 (2)		−0.2354 (5)	−0.6355 (4)	0.0625 (3)	581 (11)
S8	−0.48080 (7)	−0.53784 (5)	0.18861 (3)	170 (1)	C10	−0.4342 (3)	−0.6694 (2)	0.1039 (2)	203 (6)
	−0.47487 (10)	−0.53785 (7)	0.18954 (5)	393 (2)		−0.4303 (5)	−0.6682 (4)	0.1054 (3)	578 (11)

B. β-$(ET)_2BrICl$ at 298/120 K

atom	x	y	z	U_{eq}[a]	atom	x	y	z	U_{eq}[a]
I	0.0000	0.0000	0.0000	351 (2)	C1	−0.1428 (6)	0.2836 (4)	0.5078 (3)	264 (13)
	0.0000	0.0000	0.0000	145 (1)		−0.1378 (6)	0.2838 (4)	0.5077 (3)	118 (11)
Br	0.0899 (5)	0.2402 (3)	−0.0924 (2)	559 (11)	C2	−0.0412 (6)	0.3695 (4)	0.5865 (3)	263 (13)
	0.0822 (2)	0.2441 (1)	−0.0961 (1)	294 (3)		−0.0381 (6)	0.3698 (4)	0.5870 (3)	126 (12)
Cl	−0.0790 (5)	−0.2347 (3)	0.0912 (2)	568 (11)	C3	−0.4166 (7)	0.1440 (5)	0.3701 (3)	337 (15)
	0.0797 (2)	−0.2367 (1)	0.0931 (1)	211 (3)		−0.4128 (6)	0.1457 (4)	0.3691 (3)	132 (12)
S1	−0.4088 (2)	0.2693 (1)	0.4629 (1)	326 (4)	C4	−0.2351 (7)	0.1033 (4)	0.3612 (3)	288 (14)
	−0.4060 (1)	0.2705 (1)	0.4629 (1)	136 (3)		−0.2282 (6)	0.1042 (4)	0.3596 (3)	121 (11)
S2	−0.0138 (2)	0.1784 (1)	0.4466 (1)	337 (4)	C5	0.0497 (7)	0.5342 (4)	0.7441 (3)	276 (13)
	−0.0075 (1)	0.1775 (1)	0.4463 (1)	141 (3)		0.0519 (6)	0.5360 (4)	0.7442 (3)	125 (11)
S3	−0.1703 (2)	0.4708 (1)	0.6518 (1)	320 (4)	C6	0.2288 (7)	0.4961 (4)	0.7331 (3)	266 (13)
	0.1687 (1)	0.4718 (1)	0.6519 (1)	135 (3)		0.2328 (6)	0.4971 (4)	0.7337 (3)	114 (11)
S4	0.2251 (2)	0.3859 (1)	0.6300 (1)	320 (4)	C7	−0.6145 (8)	−0.0870 (5)	0.2730 (4)	451 (18)
	0.2307 (1)	0.3854 (1)	0.6308 (1)	136 (3)		−0.6083 (6)	−0.0876 (5)	0.2721 (4)	198 (14)
S5	−0.6616 (2)	0.0839 (2)	0.2993 (1)	553 (5)	C8	−0.4451 (8)	−0.0841 (5)	0.2088 (4)	442 (18)
	−0.6599(2)	0.0854 (1)	0.2983 (1)	221 (4)		−0.4404 (6)	−0.0825 (5)	0.2055 (3)	185 (13)
S6	−0.1880 (2)	−0.0182 (1)	0.2781 (1)	428 (4)	C9	0.2388 (9)	0.6386 (7)	0.9353 (5)	657 (25)
	−0.1809 (2)	−0.0187 (1)	0.2767 (1)	175 (3)		0.2406 (6)	0.6319 (5)	0.9387 (4)	216 (14)
S7	0.0034 (2)	0.6400 (1)	0.8392 (1)	423 (4)	C10	0.4314 (9)	0.6701 (7)	0.8912 (5)	644 (24)
	0.0044 (1)	0.6423 (1)	0.8397 (1)	174 (3)		0.4366 (6)	0.6723 (5)	0.8916 (4)	228 (14)
S8	0.4762 (2)	0.5374 (2)	0.8089 (1)	403 (4)					
	0.4827 (1)	0.5374 (1)	0.8097 (1)	168 (3)					

[a] The complete temperature factor is $\exp[-U_{eq}(\sin\theta)^2/(\lambda^2 8\pi^2)]$, where $U_{eq} = 1/3\Sigma_i\Sigma_j U_{ij} a^*_i a^*_j a_i a_j$ (in units of Å^2). Estimated standard deviations are enclosed in parentheses.

22.5 K, followed by a very abrupt drop to 4×10^{-4} emu/mol at 22 K; most of the decrease occurs between 22.2 and 22 K. Below 22 K, the derivative ESR signal intensity is very weak with a broad line width at low microwave power levels. At high power (above +20 dBm), a strong, narrow resonance is observed at 20 K, similar to the behavior reported for $(TMTSF)_2PF_6$.[27] The solid triangles at the bottom of Figure 1 indicate the peak-to-peak derivative ESR line width with the static applied field along the c^* axis. The line width is 9.8 (1) Oe at 300 K, decreases linearly with decreasing temperature to 4.7 (1) Oe at 120 K, and drops more rapidly to a minimum of 0.88 (1) Oe at 28 K. At lower temperatures a rapid increase in line width occurs, particularly between 23 and 22 K, where the spin susceptibility falls sharply while the line width rises from 2.6 (1) to 9.3 (2) Oe.

The sharp *increase* of ESR line width accompanied by an abrupt decrease in spin susceptibility between 22.5 and 22 K in β-$(ET)_2ICl_2$ (see Figure 1) is the first observation of such behavior in an ET-based synthetic metal. ESR data[28] in α-$(ET)_2I_3$ show a sudden *decrease* in both line width and spin susceptibility at a transition near 135 K, where the direct-current and microwave conductivities[13] have a pronounced drop. The ESR line width in both β-$(ET)_2I_3$ and β-$(ET)_2I_2Br$[19] decreases gradually with falling temperature between 300 and 5 K with no anomalies. ESR data for other ET-based metals such as the $(ET)_n(ReO_4)_m$ salts,[29] $(ET)_2SbF_6$,[30] and $(ET)_2AsF_6$[30] show a line width that falls with decreasing temperature or has a very slow rise by less than a factor of 2 over a broad temperature range.

In contrast, the ESR data in Figure 1 closely resemble those of pseudo-1D metals $(TMTSF)_2X$ with $X^- = PF_6^-$, AsF_6^-, and SbF_6^-,[31] which undergo metal–insulator (MI) transitions at ~ 12–15 K. The insulating states of these salts result from a spin density wave (SDW) ground state.[32] The ESR data of these $(TMTSF)_2X$ salts show a sharp increase in line width with a sharp

(27) Walsh, W. M., Jr.; Wudl, F.; Thomas, G. A.; Nalewajek, D.; Hauser, J. J.; Lee, P. A.; Poehler, T. *Phys. Rev. Lett* **1980**, *45*, 829.
(28) Venturini, E. L.; Azevedo, L. J.; Schirber, J. E.; Williams, J. M.; Wang, H. H. *Phys. Rev. B: Condens. Matter* **1985**, 32, 2819.
(29) Carneiro, K.; Scott, J. C.; Engler, E. M. *Solid State Commun.* **1984**, *50*, 477.
(30) Laversanne, R.; Amiell, J.; Delhaes, P.; Chasseau, D.; Hauw, C. *Solid State Commun.* **1984**, *52*, 177.
(31) Jerome, D.; Schultz, H. J. *Adv. Phys.* **1982**, *31*, 299 and references therein.
(32) (a) Pedersen, H. J.; Scott, J. C.; Bechgaard, K. *Phys. Rev. B: Condens. Matter* **1981**, *24*, 5014. (b) Mortensen, K.; Tomkiewicz, Y.; Schultz, T. D.; Engler, E. M. *Phys. Rev. Lett.* **1981**, *46*, 1234. (c) Andrieux, A.; Jerome, D.; Bechgaard, K. *J. Phys. Lett.* **1981**, *42*, L87.

Table IV. Bond Distances (Å) and Angles (deg) for β-(ET)$_2$ICl$_2$ and β-(ET)$_2$BrICl at 298/120 K[a]

bond	β-(ET)$_2$ICl$_2$ 298/120 K distance	β-(ET)$_2$BrICl 298/120 K distance
I-Cl	2.555 (1)/2.557 (1)	2.571 (3)/2.566 (3)
I-Br		2.638 (3)/2.647 (3)
S1-C1	1.739 (2)/1.743 (2)	1.738 (4)/1.743 (4)
S1-C3	1.749 (2)/1.752 (2)	1.750 (4)/1.749 (4)
S2—C1	1.739 (2)/1.746 (2)	1.739 (4)/1.740 (4)
S2-C4	1.756 (2)/1.755 (2)	1.751 (4)/1.749 (4)
S3-C2	1.740 (2)/1.744 (2)	1.745 (4)/1.741 (4)
S3-C5	1.760 (2)/1.761 (2)	1.758 (4)/1.758 (4)
S4-C2	1.738 (2)/1.744 (2)	1.736 (4)/1.744 (4)
S4-C6	1.751 (2)/1.752 (2)	1.754 (4)/1.758 (4)
S5-C3	1.754 (2)/1.754 (2)	1.743 (4)/1.751 (4)
S5-C7	1.811 (2)/1.820 (2)	1.810 (6)/1.814 (4)
S6-C4	1.747 (2)/1.751 (2)	1.744 (4)/1.743 (4)
S6-C8	1.810 (2)/1.827 (2)	1.814 (5)/1.826 (4)
S7-C5	1.749 (2)/1.751 (2)	1.749 (4)/1.752 (4)
S7-C9	1.798 (2)/1.817 (2)	1.804 (6)/1.818 (4)
S8-C6	1.754 (2)/1.752 (2)	1.748 (4)/1.754 (4)
S8-C10	1.806 (2)/1.816 (2)	1.814 (5)/1.819 (4)
C1-C2	1.372 (2)/1.370 (2)	1.365 (5)/1.366 (6)
C3-C4	1.341 (2)/1.355 (2)	1.350 (6)/1.364 (5)
C5-C6	1.334 (2)/1.353 (2)	1.331 (6)/1.334 (5)
C7-C8	1.509 (2)/1.510 (2)	1.520 (7)/1.531 (6)
C9-C10	1.489 (2)/1.517 (2)	1.487 (8)/1.538 (6)
bonds	**β-(ET)$_2$ICl$_2$ 298/120 K angle**	**β-(ET)$_2$BrICl 298/120 K angle**
C1-S1-C3	94.9 (1)/95.2 (1)	95.2 (2)/95.2 (2)
C1-S2-C4	95.4 (1)/95.4 (1)	95.5 (2)/95.8 (2)
C2-S3-C5	95.3 (1)/95.5 (1)	95.4 (2)/95.6 (2)
C2-S4-C6	94.9 (1)/95.2 (1)	95.2 (2)/94.9 (2)
C3-S5-C7	98.3 (1)/98.1 (1)	98.4 (2)/98.3 (2)
C4-S6-C8	102.9 (1)/102.7 (1)	103.3 (2)/103.4 (2)
C5-S7-C9	100.0 (1)/99.2 (1)	100.4 (2)/99.7 (2)
C6-S8-C10	101.2 (1)/101.1 (1)	100.9 (2)/100.7 (2)
C2-C1-S2	122.4 (2)/122.5 (2)	122.8 (3)/122.6 (3)
C2-C1-S1	122.2 (2)/122.2 (2)	121.9 (3)/122.1 (3)
S2-C1-S1	115.4 (1)/115.3 (1)	115.3 (2)/115.3 (2)
C1-C2-S3	122.2 (2)/122.5 (2)	122.8 (3)/122.8 (3)
C1-C2-S4	122.5 (2)/122.3 (2	122.3 (3)/122.2 (3)
S3-C2-S4	115.3 (1)/115.2 (1)	114.9 (2)/115.0 (2)
C4-C3-S1	117.9 (2)/117.5 (2)	126.9 (3)/117.4 (3)
C4-C3-S5	126.8 (2)/127.0 (2)	117.3 (3)/126.9 (3)
S1-C3-S5	115.3 (1)/115.5 (1)	115.7 (2)/115.7 (2)
C3-C4-S6	129.5 (2)/129.3 (2)	129.1 (3)/129.1 (3)
C3-C4-S2	116.4 (2)/116.5 (2)	116.6 (3)/116.2 (3)
S6-C4-S2	114.1 (1)/114.1 (1)	114.3 (2)/114.6 (2)
C6-C5-S7	128.5 (2)/128.1 (2)	128.4 (3)/128.2 (3)
C6-C5-S3	116.4 (2)/116.2 (2)	116.6 (3)/116.5 (3)
S7-C5-S3	115.1 (1)/115.6 (1)	115.0 (2)/115.3 (2)
C5-C6-S8	118.0 (2)/129.5 (2)	129.6 (3)/129.9 (3)
C5-C6-S4	129.3 (2)/117.7 (2)	117.7 (3)/117.8 (3)
S8-C6-S4	112.7 (1)/112.8 (1)	112.8 (2)/112.3 (2)
C8-C7-S5	112.6 (2)/112.4 (2)	112.4 (3)/112.0 (3)
C7-C8-S6	114.7 (2)/114.2 (2)	114.3 (3)/113.4 (3)
C10-C9-S7	114.8 (2)/113.0 (2)	114.2 (3)/111.8 (3)
C9-C10-S8	114.8 (2)/113.0 (2)	114.8 (3)/112.4 (3)

[a] Estimated standard deviations are in parentheses.

decrease in spin susceptibility upon lowering the temperature to their MI transition points, which is analogous to the ESR behavior of β-(ET)$_2$ICl$_2$ described above. Another similarity in the ESR properties of these two types of organic conductors is a noticeable increase in the *g* factor upon reaching the MI transition temperatures[33] [e.g., from 2.0082 (1) at 30 K to 2.0096 (1) at 22 K in β-(ET)$_2$ICl$_2$]. Thus, the insulating state of β-(ET)$_2$ICl$_2$ is likely to be caused by a SDW.

ET Molecular Structure and Network Packing

The intramolecular bond distances and angles of the ET molecules in β-(ET)$_2$ICl$_2$ and β-(ET)$_2$BrICl are given in Table IV. Previous structural analyses of (ET)$_m$X$_n$ salts have shown that much thermal motion (and positional disorder as in the case of β-(ET)$_2$I$_3$[5,7]) exist at 298 K in at least one ethylene group of the ET molecule.[8,14-19] For the ethylene carbon atoms of β-(ET)$_2$ICl$_2$ and β-(ET)$_2$BrICl, there is only a small degree of thermal motion (nearly isotropic) without any evidence of positional disorder. The complete ordering of ET molecules in β-(ET)$_2$ICl$_2$ and β-(ET)$_2$BrICl may be due to the fact that the packing of ET molecules around the anions ICl_2^- or $BrICl^-$ is more compact and more isotropic than the packing around the larger anions $X^- = I_3^-$, I_2Br^-, AuI_2^-, and IBr_2^- in other β-(ET)$_2$X salts.

The crystal packing motif of the isostructural β-(ET)$_2$X salts with small anions $X^- = ICl_2^-$ and $BrICl^-$ (referred to herein as type I salts) is significantly different from that of the isostructural salts with large anions $X^- = I_3^-$, I_2Br^-, AuI_2^-, and IBr_2^- (referred to herein as type II salts). The typical packing motifs of the 2D ET networks for types I and II salts are shown in Figure 2. A common feature of both networks is that stacks of ET molecules interact with one another to form a sheet of ET molecules in the crystallographic *ab* plane. In the ET networks of type I and II salts, a given ET molecule of one stack is positioned parallel to and between the planes of two ET molecules in an adjacent stack. This motif in type I salts is less symmetrical compared with that in type II salts, as if adjacent ET stacks are "slipped" more toward an asymmetrical arrangement for type I salts. As a consequence, short interstack S···S contacts in type I salts are found only along the crystallographic *a* axis, in contrast to the case of type II salts, which contain short S···S contacts along the *a*, *a* − *b* and *b* − *a* directions. The S···S and other intermolecular contact distances that are shorter than their associated van der Waals radii sum[34] (3.60 Å) are given in Table V. As shown in Figure 2, within each sheetlike network, an ET molecule (e.g., the ET labeled A in Figure 2) has six nearest-neighboring ET molecules (e.g., B through G). The relative orientation of ET molecules for each (i-j) pair (for i = A and j = B through G) can be described as in Figure 3,[22,35] where $R_{ij} = [(\Delta x)^2 + (\Delta z)^2]^{1/2}$ and $\phi_{ij} = \tan^{-1}$

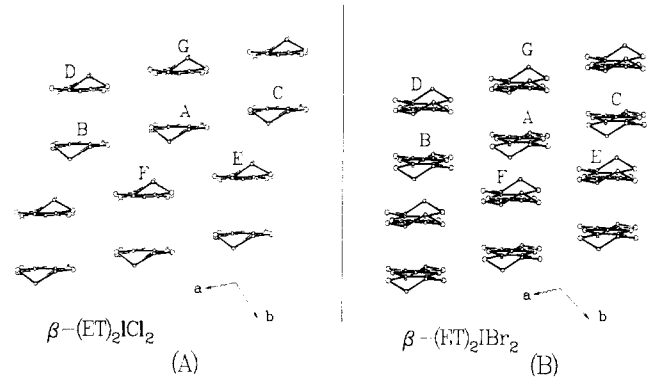

Figure 2. (A) The packing motif of ET molecules in the *ab* plane for β-(ET)$_2$ICl$_2$ is representative of type I salts. The six nearest neighbors to the central ET molecule (labeled A) are labeled B through G. (B) The analogous ET network packing motif for β-(ET)$_2$IBr$_2$ is representative of type II salts. In both cases, the view is along the normal to the *ab* plane, which is nearly along the long in-plane molecular axis of the ET molecule.

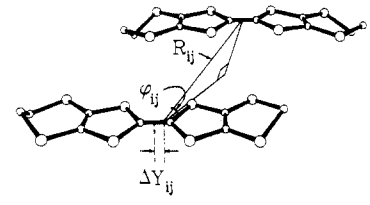

Figure 3. The relative orientation of one ET molecule to a neighboring one within a given sheetlike network can be described by the geometrical parameters R_{ij}, ϕ_{ij}, and ΔY_{ij} (see text).

(33) Torrance, J. B.; Pedersen, H. J.; Bechgaard, K. *Phys. Rev. Lett.* **1982**, *49*, 881. Walsh, W. M., Jr.; Wudl, F.; Aharon-Shalom, E.; Rupp, L. W., Jr.; Vandenberg, J. M.; Andres, K.; Torrance, J. B. *Phys. Rev. Lett.* **1981**, *49*, 885.

(34) Pauling, L. "The Nature of the Chemical Bond" Cornell University Press: Ithaca, NY, 1960.

Table V. Interatomic Distances between Molecules in β-$(ET)_2ICl_2$ and β-$(ET)_2BrICl$ Less Than the van der Waals Sum[a]

contact	β-$(ET)_2ICl_2$	β-$(ET)_2BrICl$	
	A. S···S Contact Distances (Å) between ET Molecules[b] at 298/120 K		
S7···S8	3.445 (1)/3.416 (1)	3.453 (1)/3.421 (1)	
S5···S6	3.454 (1)/3.421 (1)	3.457 (1)/3.425 (1)	
S3···S8	3.536 (1)/3.504 (1)	3.536 (1)/3.506 (1)	
S2···S5	3.542 (1)/3.507 (1)	3.535 (1)/3.497 (1)	
	B. X···S Contacts at 298/120 K		
Cl···S6	3.490 (1)/3.441 (1)	3.540 (1)/3.480 (3)	
Br···S6		3.535 (3)/3.494 (3)	
		β-$(ET)_2BrICl$	
contact	β-$(ET)_2ICl_2$	Cl	Br[c]
	C. X···H Distances that Surround the Anion X^- at 120 K[d]		
Cl···H7B	2.59	2.61	2.62
Cl···H10A	2.64	2.66	2.65
Cl···H9A	2.78	2.78	2.79
Cl···H8B	2.88	2.92	2.90
Cl···H9B	2.91	2.69	2.90

[a] Associated van der Waals radii (Å) are 1.25 for H, 1.80 for Cl, 1.80 for S, and 1.95 for Br. Therefore, the van der Waals contact distances (Å) are 3.05 for H···Cl, 3.20 for H···Br, 3.60 for S···S, 3.60 for S···Cl, and 3.75 for S···Br.[34] [b] The short S···S contacts here are between ET molecules related by a unit cell translation along the *a* axis. [c] The spatial separation between a given Cl atom and the inversion mate for Br for the same $BrICl^-$ anion in β-$(ET)_2BrICl^-$ is less than 0.1 Å. [d] See Figure 5. The C–H bonds have the internuclear distance of 1.09 Å.[26]

$(\Delta z/\Delta x)$, given the displacement of molecule j with respect to molecule i as $(\Delta x, \Delta y, \Delta z)$ in the local Cartesian system defined in **1**. The R_{ij}, ϕ_{ij}, and ΔY_{ij} values for the six ET pairs (i-j) in type I and II salts are listed in Table VI. Also listed in Table VI are the HOMO interaction energies $\beta_{ij} = \langle\psi_i|H^{eff}|\psi_j\rangle$, where ψ_i and ψ_j are the HOMO's of molecules i and j, respectively.[36] These interaction energies are important for characterizing the valence (i.e., highest occupied) bands of the type I and II salts and hence for understanding their electrical properties. From Figure 2 and Table VI, we note the following observations concerning the packing modes of ET molecules in type I and II salts:

(a) Within a given stack, ET *dimers* (e.g., the A-G pair in Figure 2) propagate along the $a + b$ direction. The magnitude of interaction within this dimeric unit, as measured by the $\beta_{A\text{-}G}$ values in Table VI, is comparable for both type I and II salts. However, the magnitude of interaction *between* dimeric units as measured by $\beta_{A\text{-}F}$ values in Table VI is much smaller for the type I salts compared to the type II salts.

(b) Between the ET stacks in either type I or type II salts there are four pairwise interactions, namely A-B, A-C, A-D, and A-E (see Figure 2). The magnitudes of these *inter*stack interactions for the type I and II salts are comparable, despite the fact that the relative arrangement of adjacent stacks is significantly different for type I vs. type II salts. Thus, in type I salts, interactions between ET dimers along a given stack are extremely weak compared to interstack interactions. Consequently, the ET network of type I salts is not expected to be 2D metallic, as in type II salts. As a further consequence of our findings, it appears likely that trihalide anions shorter in length than ICl_2^-, such as those that contain fluorine atoms, will likely mimic the type I salt behavior and be 1D metallic in nature.

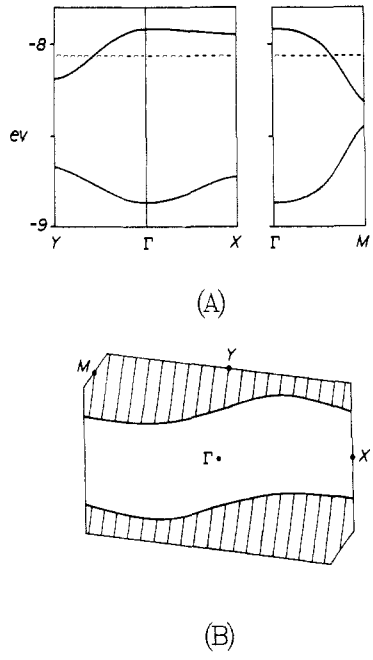

Figure 4. (A) Dispersion relations for the two highest occupied bands of β-$(ET)_2ICl_2$ at 120 K, where the dashed line refers to the Fermi level. Γ, *X*, *Y*, and *M* represent the wavevector points (0, 0), $(a^*/2, 0)$, $(0, b^*/2)$, and $(-a^*/2, b^*/2)$ of the first Brillouin zone, respectively. The curves corresponding to the 298 K structure of β-$(ET)_2ICl_2$ and the 298 and 120 K structures of β-$(ET)_2BrICl$ are nearly identical with the ones shown. (B) The Fermi surface of β-$(ET)_2ICl_2$ at 120 K associated with the upper band of Figure 4A. The wavevectors in the shaded and unshaded regions of the first Brillouin zone lead to the occupied and unoccupied levels of this band, respectively. The boundary separating these two regions, i.e., the Fermi surface, is not closed.

Band Electronic Structure

To examine the electrical properties of β-$(ET)_2ICl_2$ and β-$(ET)_2BrICl$, tight-binding band electronic structure calculations[36,37] were performed and were based on the crystal structures of these salts at 298 and 120 K. To better describe the inter- and intrastack interactions between ET molecules, the valence orbitals of carbon and sulfur atoms were represented by double-ζ Slater type orbitals.[36,37] Figure 4A shows the dispersion of the highest two occupied bands for the 120 K structure of β-$(ET)_2ICl_2$. The band electronic structures for the 298 K structure of β-$(ET)_2ICl_2$ and the 120 and 298 K structures of β-$(ET)_2BrICl$ are all very similar to that shown in Figure 4A. The orbital character of these two bands is largely composed of the HOMO of each ET molecule. Given the bonding and antibonding combinations of the HOMO's of each ET dimer as ψ_+ and ψ_-, respectively, the lower and upper bands of Figure 4A are mainly based upon ψ_+ and ψ_-, respectively. Because of the formal oxidation $(ET)_2^+$, there are three electrons per unit cell for the two bands so that the upper band (i.e., the valence band) is half-filled. It is noted here that the valence band is dispersive along the $\Gamma \rightarrow Y$ or $\Gamma \rightarrow M$ direction, but flat along the $\Gamma \rightarrow X$ direction. Consequently, the Fermi surface (see Figure 4B) calculated for β-$(ET)_2ICl_2$ is open, and this salt is a 1D metal. This result is consistent with our ESR observation that, in one direction within the ET network plane, the microwave conductivity is low. Previous band electronic structure calculations for the type

Table VI. Interaction Parameters for ET Molecules in Type I and II Salts at 120 K[a]

	β_{ij}, eV		R_{ij}, Å		ϕ_{ij}, deg		ΔY_{ij}, Å	
i-j pair	I	II	I	II	I	II	I	II
A-B[b]	0.057	0.012	6.40	6.31	-10.8	-12.7	-1.57	-1.88
A-D	0.089	0.075	6.62	6.47	18.8	17.2	-0.28	-0.27
A-E	0.198	0.167	5.33	6.14	38.7	23.5	-4.21	-1.93
A-F[c]	0.014	0.325	5.01	3.88	-64.8	-82.2	-5.88	-3.81
A-G	0.522	0.490	3.34	3.31	89.6	89.6	1.39	1.61

[a] Type I salts are typified here by β-$(ET)_2ICl_2$ and type II by $\beta(ET)_2IBr_2$. [b] ET molecules A through G are pictured in Figure 2. The A-B pairwise interaction is equivalent to A-C by translation. [c] Note the highly contrasting values for only A-F pairs.

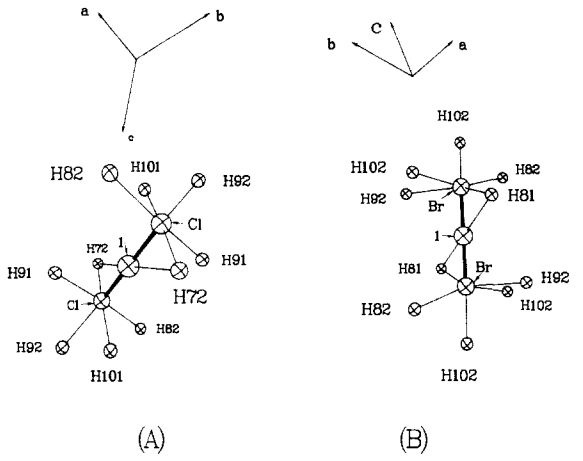

Figure 5. (A) A perspective view of the arrangement of H atoms that surround the ICl_2^- anions in β-$(ET)_2ICl_2$ at 120 K. All C–H distances are set to 1.09 Å. (B) The corresponding arrangement for type II salts is represented by that in β-$(ET)_2IBr_2$ at 120 K. For both motifs, there is a common quintet of close H···X distances (i.e., H···Br distances less than 3.2 Å and H···Cl distances less than 3.0 Å).

II β-$(ET)_2X$ salts with $X^- = I_3^-$ and IBr_2^- have shown that these salts, which have longer anions (compared to type I salts), are 2D metals.[22,35,37]

It is known that many other 1D organic metals undergo MI transitions upon lowering the temperature.[38] The low-temperature insulating states of 1D materials may be either diamagnetic or magnetic in nature.[31,39] The crystal structures of the pseudo-1D metal $(TMTSF)_2PF_6$ that were determined above[40] and below[41] its phase transition (T_{MI} = 12 K) reveal no evidence of a superlattice below T_{MI}. This result agrees with other experimental findings[32] that the insulating state of $(TMTSF)_2PF_6$ below T_{MI} is a SDW state and not a CDW state or a new crystallographic phase. Axial rotation photographs of the X-ray diffraction intensities about the *a*, *b*, and *c* axes in β-$(ET)_2ICl_2$ at ~15 K[42] (i.e., at a temperature below its phase transition at ~22 K), revealed no evidence of superlattice formation. From this result and the facts that the ESR behaviors of β-$(ET)_2ICl_2$ and $(TMTSF)_2PF_6$ are similar and that both are pseudo-1D metals, it is probable that the insulating state of β-$(ET)_2ICl_2$ is also a SDW state. A result similar to that found for β-$(ET)_2I_2Br$[19a] (i.e., electrical behavior governed by its anion disorder) is predicted for β-$(ET)_2BrICl$.

ET–Anion Interactions

It is important to examine why two types of ET networks occur in β-$(ET)_2X$ salts with trihalide anions X^-, which may be discussed from the viewpoint of packing interactions between the anions and the ET molecules that surround them, especially those of the H···X type. The disorder of the asymmetric $BrICl^-$ anion, which results from the inversion symmetry imposed on this molecule by the lattice and also from compositional disorder for the Br and Cl atoms (vide supra), prohibits the assignment of H···X interactions unambiguously to H···Br or H···Cl. Thus, the ET–anion interactions will not be discussed for β-$(ET)_2BrICl$ except to state that its completely ordered ET molecules and ET network, which are influenced by these H···X interactions, are nearly identical with those in β-$(ET)_2ICl_2$. Also, because of anion disorder (as in β-$(ET)_2I_2Br$[19]) the $X^- = BrICl^-$ derivative is not expected to be an ambient-pressure superconductor. As listed in Table V, each terminal halogen atom of X^- in type I or II salts makes short H···X contacts (less than or equal to the van der Waals radii sum) with the ethylene groups of the surrounding ET molecules. In type I and II salts, each terminal halogen atom of X^- is surrounded by many H atoms, five of which are very close to the terminal halogen, as shown in Figure 5. This seems to be a general packing pattern in both types of salts for the ET molecules in the immediate vicinity of the terminal halogen. Consequently, the relative arrangement of ET pairs within a stack and between adjacent stacks (e.g., a "slipping" along the $a + b$ direction, as in Figure 2) will sensitively depend upon the length of the trihalide anion X^-. Therefore, the entire ET network, and hence its band electronic structure, can be considered to be strongly influenced by the packing interaction of ET molecules around the anion X^-.

Summary and Concluding Remarks

We have synthesized the new organic metals β-$(ET)_2ICl_2$ and β-$(ET)_2BrICl$ and determined their crystal structures at 298 and 120 K. Our ESR measurements on β-$(ET)_2ICl_2$, and band electronic structure calculations on β-$(ET)_2ICl_2$ and β-$(ET)_2BrICl$, show that these salts (referred to here as type I salts) are 1D metals, in contrast to the β-$(ET)_2X$ salts with larger anions, $X^- = I_3^-$, I_2Br^-, IBr_2^-, and AuI_2^- (type II salts), which are 2D metals. The ESR microwave conductivity of β-$(ET)_2ICl_2$ shows a metal–insulator transition at ~22 K. All of the ESR characteristics of β-$(ET)_2ICl_2$ around the transition temperature are very similar to those of the pseudo-1D metal $(TMTSF)_2PF_6$, which is known to undergo a metal–SDW transition. Thus, the insulating state of β-$(ET)_2ICl_2$ is probably due to a SDW as well. The β-$(ET)_2BrICl$ salt likely remains metallic to low temperatures, if its electrical behavior resembles β-$(ET)_2I_2Br$, which also contains disordered anions in its structure.

In order to understand the structural basis for the different electronic properties of type I and II salts, we examined the relative arrangements and the HOMO interaction energies between pairs of nearest-neighbor ET molecules in their planar ET networks. According to these results, interactions *between* dimeric ET units in a given stack are extremely weak for type I salts, unlike the case for type II salts. This difference in ET network motif between type I and type II salts was analyzed on the basis of packing interactions between ET molecules and anions. Common to both type I and II salts, the packing of ET molecules around each terminal halogen atom of X^- appears to require five short H···X contacts. Thus, the relative arrangement of ET pairs within a stack and between adjacent stacks can be altered by varying the length of the anion X^-. An important consequence of the packing interactions between ET molecules and anions with regard to the ET network is that the β-$(ET)_2X$ salts with small anions ($X^- = ICl_2^-$ and $BrICl^-$) are 1D metals and those with large anions ($X^- = I_3^-$, I_2Br^-, IBr_2^-, and AuI_2^-) are 2D metals. Finally, the search for new ambient-pressure organic superconductors in the β-$(ET)_2X$ class should center on linear anions of length greater than that of IBr_2^- (but perhaps less than that of I_3^-).

Acknowledgment. Work at Argonne National Laboratory and Sandia National Laboratories is sponsored by the US Department of Energy (DOE), Office of Basic Energy Sciences, Division of Materials Sciences, under Contracts W-31-109-Eng-38 and KC020202, respectively. We thank D. L. Overmyer for his expert technical assistance. P.R.R., J.D.C., and P.L.J. are student research participants sponsored by the Argonne Division of Edu-

(35) Mori, T.; Kobayashi, A.; Sasaki, Y.; Kobayashi, H.; Saito, G.; Inokuchi, H. *Chem. Lett.* **1984**, 957. Mori, T.; Kobayashi, A.; Sasaki, Y.; Kobayashi, H.; Saito, G.; Inokuchi, H. *Bull. Chem. Soc. Jpn.* **1984**, *57*, 627.

(36) Our tight binding band calculations were based upon the extended Hückel method: Hoffmann, R. *J. Chem. Phys.* **1963**, *39*, 1397. We used double-ζ Slater type orbitals adapted from: Clementi, E.; Roetti, C. *At. Data Nucl. Data Tables* **1974**, *14*, 177. The $H_{\mu\nu}$ values were calculated from a modified Wolfsberg–Helmholtz formula: Ammeter, J. H.; Bürgi, H. B.; Thibeault J. C.; Hoffmann, R. *J. Am. Chem. Soc.* **1978**, *100*, 3686. See ref 22 for details.

(37) Whangbo, M.-H.; Williams, J. M.; Leung, P. C. W.; Beno, M. A.; Emge, T. J.; Wang, H. H.; Carlson, K. D.; Crabtree, G. W. *J. Am. Chem. Soc.* **1985**, *107*, 5815.

(38) Bechgaard, K.; Jacobsen, C. S.; Mortensen, K.; Pedersen, H. J.; Thorup, N. *Solid State Commun.* **1980**, *33*, 119.

(39) Whangbo, M.-H. From "Crystal Chemistry and Properties of Materials with Quasi One-Dimensional Structures"; Rouxel, J., Ed.; Reidel; Dordrecht, 1985; pp 27–85.

(40) Thorup, N.; Rindorf, G.; Soling, H. *Acta Crystallogr. Sect. B: Struct. Crystallogr. Cryst. Chem.* **1981**, *B37*, 1236.

(41) Gallois, B.; Gaultier, J.; Hauw, C.; Chasseau, D.; Meresse, A.; Filhol, A.; Bechgaard, K. *Mol. Cryst. Liq. Cryst.* **1985**, *119*, 225.

(42) Cell data from single crystal X-ray diffraction at ~15 K are space group $P\bar{1}$; $Z = 1$; $a = 6.56$ (2) Å; $b = 9.59$ (2) Å; $c = 12.81$ (2) Å; $\alpha = 86.4$ (1)°; $\beta = 100.1$ (2)°; $\gamma = 97.2$ (2)°; $V = 786$ (3) Å^3.

cational Programs from the University of Wisconsin, Eau-Claire, Carnegie-Mellon University (Pittsburgh, PA) and Cumberland College (Kentucky), respectively. This work is in part supported by the Camille and Henry Dreyfus Foundation through a Teacher-Scholar Award to M.-H. Whangbo. The authors express their appreciation for computing time on the ER-Cray computer, made available to us by the DOE.

Supplementary Material Available: Tables of refined anisotropic thermal parameters for all non-hydrogen atoms, hydrogen atom fractional coordinates, least-squares planes through the ET molecules, the calculated H-atom positions and lists of observed and calculated structure factors for β-$(ET)_2ICl_2$ and β-$(ET)_2BrICl$ at 298 and 120 K (102 pages). Ordering information is given on any current masthead page.

Heat Capacity and Phase Transitions of the Mixed-Valence Compound $[Fe_3O(O_2CCH_3)_6(py)_3](py)$[1]

Michio Sorai,*† Kazutoshi Kaji,† David N. Hendrickson,*‡ and Seung M. Oh‡

Contribution from the Chemical Thermodynamics Laboratory, Faculty of Science, Osaka University, Toyonaka, Osaka 560, Japan, and the School of Chemical Sciences, University of Illinois, Urbana, Illinois 61801. *Received July 19, 1985*

Abstract: The heat capacity under constant pressure, C_p, of oxo-centered mixed-valence $[Fe_3O(O_2CCH_3)_6(py)_3](py)$ has been measured with an adiabatic calorimeter between 12 and 300 K. Four phase transitions were found to occur at 111.4, 112.0, 185.8, and 191.5 K. These transitions can be classified basically into two groups: one is a lower-temperature phase transition with two C_p peaks in the 111-112 K region and the other is a higher-temperature phase transition evolving from ~115 K to culminate in two C_p peaks in the 185-191 K region. The total enthalpy and entropy of these phase transitions were determined by estimating plausible normal heat capacities to give 4940 J mol^{-1} and (30.58 ± 0.83) J K^{-1} mol^{-1}, respectively. By comparing the present results with the ^{57}Fe Mössbauer spectroscopy and the X-ray structural work reported for this complex, it is concluded that these phase transitions are associated with the *intra*molecular electron transfer in the mixed-valence Fe_3O complexes and the orientational disordering of the pyridine solvate molecules about the crystallographic C_3 axis. DTA data for the solid solutions, $[Fe^{III}_2Fe^{II}_{1-x}Co^{II}_xO(O_2CCH_3)_6(py)_3](py)$, indicate that the phase transition having a C_p peak at 185.8 K is due to the orientational order-disorder phenomenon associated with the pyridine solvate molecules. The observed transition entropy is much larger than the value (R ln 3) expected to result from electronic delocalization in the $Fe^{III}_2Fe^{II}$ triads and the orientational disorder (R ln 3) about the C_3 axis of the pyridine solvate molecules. Two possibilities to account for the remaining entropy are discussed: one is associated with changes in the orbital degeneracy of the Fe(II) ion and the other is the rotation of the pyridine solvate molecules about their pseudo-C_6 axes.

A variety of transition-metal compounds are known to change their electronic states in the solid state as the result of a change in temperature. Among them, mixed-valence complexes form one class; other examples are spin-crossover complexes[6-8] and complexes exhibiting thermochromism.[9] These compounds often exhibit interesting phase-transition phenomena, in which the change in electronic states is strongly coupled with a change in their phonon systems.

The present compound, μ_3-oxo-tris(pyridine)hexakis(acetato)iron(II)-diiron(III)monopyridine, $[Fe_3O(OAc)_6(py)_3](py)$, is a typical example of a trinuclear, oxo-centered mixed-valence iron acetate complex. Variable-temperature ^{57}Fe Mössbauer spectroscopy[10,11] for this compound has revealed interesting features characteristic of an *intra*molecular electron transfer, and suggesting a phase transition between the electron-localized and -delocalized states. Preliminary X-ray structural work[12] showed that $[Fe_3O(OAc)_6(py)_3](py)$ crystallizes in the space group $R32$ at room temperature, where there are stacks of Fe_3O complexes with a C_3 axis running down each stack. Recent ongoing X-ray structural work[13] shows that the pyridine solvate molecules, which have their molecular planes oriented perpendicular to the Fe_3O planes, are orientationally disordered in three positions about the C_3 axis at room temperature, whereas this symmetry axis disappears at low temperatures. On the basis of these experiments, two of the present authors and their collaborators[10,11] have emphasized the importance of a significant coupling between the motional state of the pyridine solvate molecule and the *intra*molecular electron-transfer rate in the Fe_3O complex.

Thermodynamic studies, in particular heat capacity measurements, serve as a powerful tool to elucidate energetic and entropic aspects of a phenomenon, from which one can obtain definitive evidence as to whether a phase transition exists or not. Moreover, based on the transition entropy, it is possible to discover microscopic processes which are involved in a phase transition that spectroscopic and structural studies fail to detect. One of the objectives of the present paper is to combine macroscopic entropic aspects complementarily with the microscopic aspects derived from spectroscopic and structural data. To this end, heat capacity measurements were made in the range from 12 to 300 K for $[Fe_3O(OAc)_6(py)_3](py)$. It will be shown that there are four phase

† Osaka University.
‡ University of Illinois.

(1) Contribution No. 90 from the Chemical Thermodynamics Laboratory.
(2) Day, P *Int. Rev. Phys. Chem.* **1981**, *1*, 149.
(3) "Mixed-Valence Compounds: Theory and Applications in Chemistry, Physics, Geology and Biology"; Brown, D. B., Ed.; D. Reidel: New York, 1980.
(4) Creutz, C. *Prog. Inorg. Chem.* **1983**, *30*, 1.
(5) Richardson, D. E.; Taube, H. *Coord. Chem. Rev.* **1984**, *60*, 107.
(6) König, E. *Ber. Bunsenges. Phys. Chem.* **1972**, *76*, 975.
(7) Goodwin, H. A. *Coord. Chem. Rev.* **1976**, *18*, 293.
(8) Gütlich, P. *Struct. Bonding* **1981**, *44*, 83.
(9) Day, J. H. *Chem. Rev.* **1963**, *63*, 65.
(10) Oh, S. M.; Hendrickson, D. N.; Hassett, K. L.; Davis, R. E. *J. Am. Chem. Soc.* **1984**, *106*, 7984.
(11) Oh, S. M.; Hendrickson, D. N.; Hassett, K. L.; Davis, R. E. *J. Am. Chem. Soc.*, in press.
(12) See Table III in: Catterick, J.; Thornton, P. *Adv. Inorg. Chem. Radiochem.* **1977**, *20*, 291. Where it is indicated that $[Fe_3O(OAc)_6(py)_3](py)$ is isostructural to the analogous manganese compound, the structure of which has been communicated: Baikie, A. R. E.; Hursthouse, M. B.; New, D. B.; Thornton, P. *J. Chem. Soc., Chem. Commun.* **1978**, 62.
(13) Strouse, C. E.; Hendrickson, D. N.; Oh, S. M., unpublished results.

0002-7863/86/1508-0702$01.50/0